

Dislocation flow turbulence simultaneously enhances strength and ductility

Yang Chen^a 📵, Hui Feng^a 📵, Jia Li^{a,1} 📵, Bin Liu^b, Chao Jiang^a 📵, Yong Liu^b, Qihong Fang^{a,1} 📵, and Peter K. Liaw^c 📵

Edited by Alexis Bell, University of California, Berkeley, CA; received September 29, 2023; accepted January 25, 2024

Multi-principal element alloys (MPEAs) exhibit outstanding strength attributed to the complex dislocation dynamics as compared to conventional alloys. Here, we develop an atomic-lattice-distortion-dependent discrete dislocation dynamics framework consisted of random field theory and phenomenological dislocation model to investigate the fundamental deformation mechanism underlying massive dislocation motions in body-centered cubic MPEA. Amazingly, the turbulence of dislocation speed is identified in light of strong heterogeneous lattice strain field caused by short-range ordering. Importantly, the vortex from dislocation flow turbulence not only acts as an effective source to initiate dislocation multiplication but also induces the strong local pinning trap to block dislocation movement, thus breaking the strength-ductility trade-off.

dislocation flow turbulence | chemical short-range order | strength and ductility | vortex | multi-principal element alloy

The frequent changes of atom type and size cause a large atomic-scale lattice distortion in multi-principal element alloys (MPEAs), resulting in excellent mechanical properties, such as great strength and good ductility (1-3), and high fracture toughness (4, 5). In particular, refractory MPEA (RMPEA) shows high strength at elevated temperatures (6), but its low room-temperature ductility hinders the wide applications (6). Recently, non-screw dislocation slip plays an important contribution to plastic deformation in RMPEA (7) and attracts a lot of great attention to break through this dilemma (8). Additionally, the differences of the electronic interactions lead to the existence of preference or avoidance in the atom bonding and then produce chemical short-range order (SRO) to reduce the free energy of the system confirmed by experiments (9-11). Considering the fact that stacking fault, twinning, and phase transformation are the dislocation-mediated process (9, 11), the SRO-induced non-uniform lattice strain fields result in unusual dislocation behavior for the excellent performance compared to traditional alloys (10, 12). Moreover, SRO is a highly adjustable parameter to design MPEA with excellent performance based on the regulation of processing condition and alloy composition (13). Therefore, a deeper understanding of interaction between SRO and dislocation would provide insights into the development of excellent MPEAs. However, the influence of the collective dislocation movement on ductility and hardening at the micrometer scale remains undisclosed in severely distorted body-centered cubic (bcc) crystals.

Here, we develop a continuum random field model using a three dimentional (3D) strain-field function obtained by the Weierstrass-Mandelbrot fractal method to fit the lattice strain field in a model HfNbTa RMPEA and then import this model into discrete dislocation dynamics (DDD) simulation (Fig. 1 and SI Appendix, Tables S1-S4), which formally interrelate the dislocation multiplication, dislocation plasticity, and dislocation hardening (SI Appendix, Text 1 and Figs. S1-S3). On the one hand, HfNbTa RMPEA exhibits high strength and excellent tensile ductility, which has great potential in engineering applications as structural materials (14). On the other hand, the one-element segregation promotes the adjacent arrangement of the other two elements, which is beneficial for the direct observation of SRO in the ternary HfNbTa. For example, the previous pioneer work also adopts the same strategies to characterize the degree and spatial extent of local chemical ordering configuration in the CrCoNi and CoNiV MPEAs studied experimentally (10, 12). Thus, HfNbTa RMPEA as the model alloy is investigated. The overlap calculation process is as follows: Based on the Monte Carlo/molecular dynamics (MC/MD) simulation, the heterogeneous lattice strain field caused by SRO in a model HfNbTa RMPEA is obtained (Fig. 1A and SI Appendix, Text 1). The dislocation mobility is obtained through phenomenological dislocation mobility model and the velocity of a single dislocation from MD simulations (Fig. 1B). Then, a continuum random field model is developed by using a 3D strain-field function derived from a two-dimensional Weierstrass-Mandelbrot fractal method, to fit the lattice strain field (Fig. 1C and SI Appendix, Text 1). This 3D strain-field function is transferred to the DDD simulation

Significance

Improving both the strength and ductility of metal materials has always been a great challenge for a long time. Our work shows the underlying physical characteristics of chemical short-range order in multiprincipal element alloys, which causes higher strain peaks and wider strain wavelengths compared to traditional alloys. Remarkably, the heterogeneous lattice strain field induces a unique dislocation turbulent behavior and forms a special dislocation structure that is both a source and a trap at the vortex point, significantly enhancing both strength and ductility. This provides a clear adjustable parameter for the design of high-strength and ductile metal

Author affiliations: aCollege of Mechanical and Vehicle Engineering, Hunan University, Changsha 410082, People's Republic of China; ^bState Key Laboratory of Powder Metallurgy, Central South University, Changsha 410083, People's Republic of China; and ^cDepartment of Materials Science and Engineering, The University of Tennessee, Knoxville, TN 37996

Author contributions: J.L. and Q.F. designed research; Y.C., H.F., J.L., and Q.F. performed research; Y.C., H.F., J.L., B.L., C.J., Y.L., Q.F., and P.K.L. analyzed data; and Y.C., J.L., B.L., C.J., Y.L., Q.F., and P.K.L. wrote the paper.

The authors declare no competing interest.

This article is a PNAS Direct Submission.

Copyright © 2024 the Author(s). Published by PNAS. This article is distributed under Creative Commons Attribution-NonCommercial-NoDerivatives License 4.0

¹To whom correspondence may be addressed. Email: lijia123@hnu.edu.cn or fangqh1327@hnu.edu.cn.

This article contains supporting information online at https://www.pnas.org/lookup/suppl/doi:10.1073/pnas. 2316912121/-/DCSupplemental.

Published March 19, 2024.

to explore the unusual dislocation motion and flow turbulence in severely distorted bcc crystals.

To investigate the effect of SRO on the strengthening behavior of bcc MPEA, two simulation samples including an as-cast random solid solution and an annealed state are presented using MD simulation and hybrid MD/MC approach (SI Appendix, Figs. S1 and S2). Clearly, the resulting SRO shows clear segregation of the Ta-Ta elements (Fig. 2A and SI Appendix, Fig. S3), agreeing with a recently reported experimental investigation (15). The associated atomic strain suggests that SRO causes the strong strain accumulation (Fig. 2B), especially the element-segregated regions. Wherein, the Ta enrichment induces the local tensile strain, while on the contrary, the enrichment of Hf and Nb promotes the local compressive strain (Fig. 2A). The strain from MD simulation fluctuates within the range of from -5 to 5% (Fig. 2B), which has the same magnitude as the previous experiments in MPEAs (11). To reveal the nature of SRO on lattice strain, the strain rms is analyzed. The power correlation between the rms and scan size is found (Fig. 2C and SI Appendix, Fig. S4) (16), in accordance with the characteristic of the residual strain field reported experimentally in other MPEAs (17, 18). Then, a strain-field function is constructed by the fractal method for extending the atomic scale strain field obtained by MD to a continuous infinite space (Fig. 1). Since the dislocations could be blocked at the position of strain peaks, the spatial distribution of strain peaks would determine their motion behaviors. Here, the minimum spacing

tree connection diagram is used to evaluate the spatial-distribution dispersion degree of strain peaks (*SI Appendix*, Fig. S5) (19–21). The same average and SD in the strain-peak spacing between the strain fields from the MD simulation and theoretical model indicate a good accuracy for the extended strain field (*SI Appendix*, Fig. S5).

Interestingly, the power relationship disappears with the increase of scanning size. It suggests that a maximum cutoff wavelength for a strain field caused by the deviatoric-part of lattice distortion only exists at several nanometers, and the chemical SRO enhances a maximum cutoff wavelength and the incidence (Fig. 2 B and C) (16, 22). Here, the strain field of the MPEA is obtained by superposition of every atomic strain field using the Eshelby approach (19). The nanoscale strain wave is consistent with the elemental concentration wavelength (Fig. 2 A and B), which is confirmed by the experiment using aberration-corrected TEM imaging (10-12). Hence, the elemental enriched clusters get together to induce a large wavelength strain field when SRO exists (10, 20). The variation of strain wavelength with the SRO degree is measured, and it indicates a positive correlation between strain wavelength and SRO (SI Appendix, Fig. S6A). Furthermore, the strain wavelength increases dramatically at the high SRO degree (SI Appendix, Fig. S6B). This result indicates that SRO improves the upper limit of the strain wavelength in the annealed sample.

To assess the impact of SRO on mechanical response, the stressstrain curve is presented (Fig. 3A). As expected, the yield strength

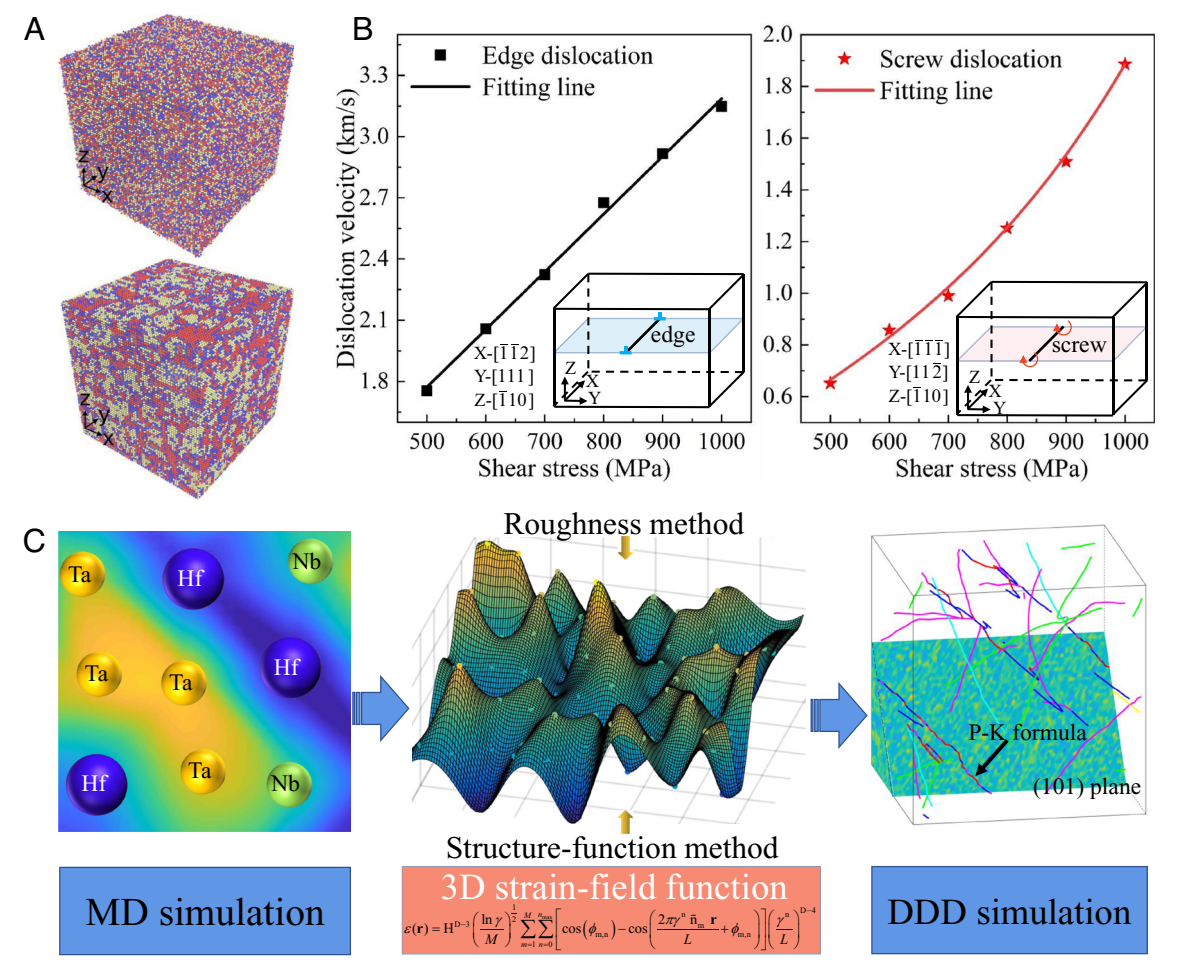


Fig. 1. Cross-scale simulation from atomic scale SRO to mesoscopic scale DDD. (*A*) The atomic model of HfNbTa RMPEA without and with SRO. Here, ● Hf, ● Nb, and ○ Ta. (*B*) Dislocation velocity as a function of the applied shear stress for edge and screw dislocations. (*C*) Schematic diagram of the atomic lattice-distortion-dependent DDD simulation framework.

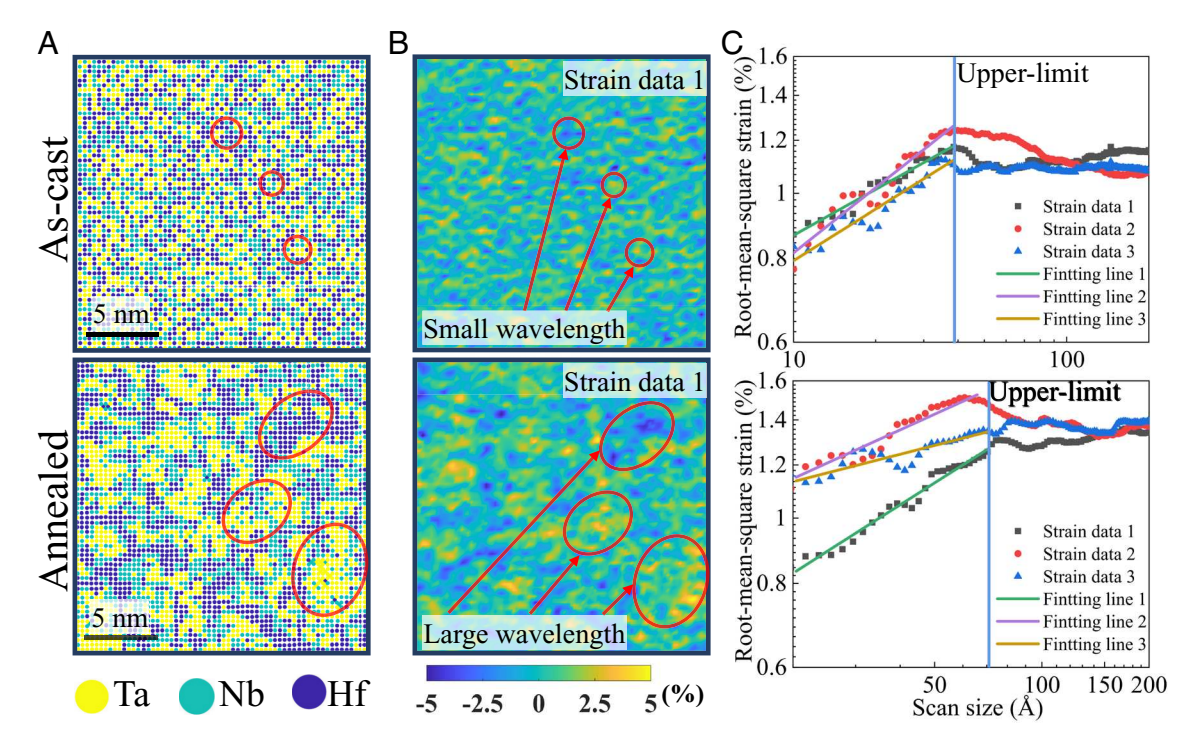


Fig. 2. Characterization of lattice distortion induced by chemical SRO. (*A*) The atomic configurations colored according to the element types in a random solid solution and an annealed sample. (*B*) The distribution of residual normal strain viewed along the [100] direction. (*C*) The rms of residual strain vs. scan size in log-log plot.

of the HfNbTa RMPEA with SRO is larger than that in as-cast sample (Fig. 3A), where the corresponding strength corresponds to the stress obtained from the 0.2% strain (23, 24). This is owing to that a high lattice strain peak induced by SRO hinders dislocation slip (25, 26). Thus, SRO is regarded as a valve to hinder dislocation movement and then leads to a large shear stress required for dislocation to break through obstacles. Moreover, the strain hardening rate increases in the annealed sample during the plastic deformation stage, which indicates that MPEA with SRO has both high strength and ductility (Fig. 3A).

The dynamic evolution of microstructure shows that excellent mechanical properties depend on the increasing density of movable/immovable dislocations (Fig. 3B and SI Appendix, Figs. S7 and S8). The immovable dislocations hinder subsequent dislocation movement to increase strain hardening, while the movable dislocations generate the ductility through their movement (18). This is clearly observed that a large number of dislocations pile-up in the local areas to produce immovable dislocation tangle, highlighted in the red circle (Fig. 3B). The proliferation and accumulation of dislocations are closely related to the bidirectional transformation between

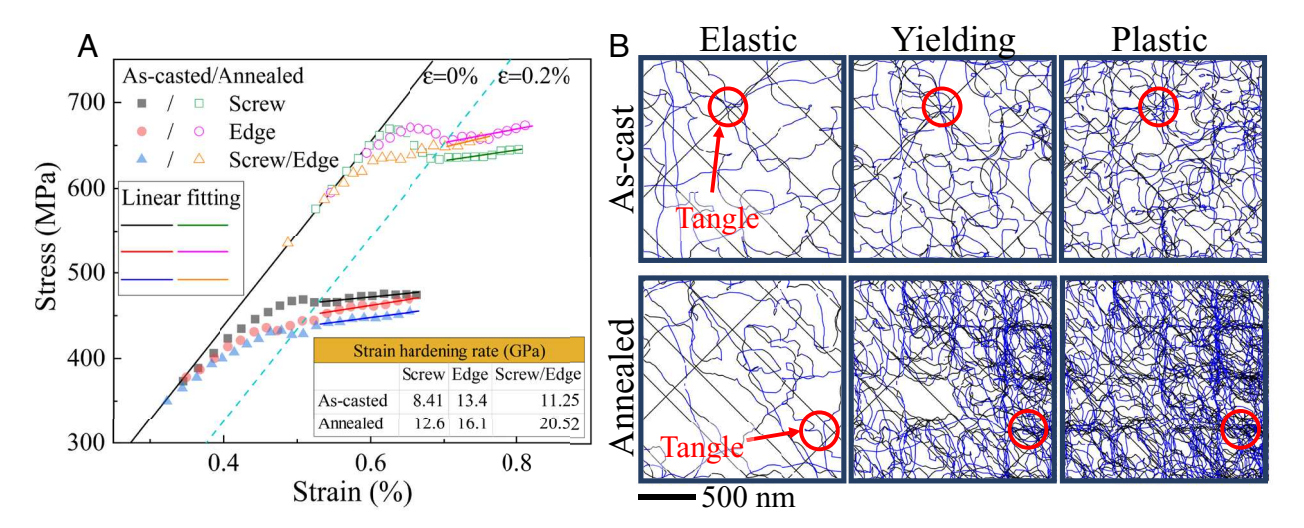


Fig. 3. Effect of SRO on mechanical properties of HfNbTa RMPEA. (*A*) The stress vs. strain of the HfNbTa for the as-cast and annealed samples. To avoid the randomness related to the initially built model, three different initial dislocation structures are considered. Here, the "Screw", "Edge", and "Screw/Edge" are the initial structure with screw dislocation, edge dislocation, and the coexistence of screw and edge dislocation. The strain hardening rate is obtained by linearly fitting the plastic strain-stress data after the yield point. (*B*) Movable/immovable dislocation distribution marked by blue/black line for as-cast sample at the elastic (ϵ = 0.3%), yielding (ϵ = 0.5%) and plastic (ϵ = 0.6%) stages and annealed sample at the elastic (ϵ = 0.5%), yielding (ϵ = 0.7%), and plastic (ϵ = 0.8%) stages, with initial screw and edge dislocation structure.

screw and edge dislocations, where this bidirectional transformation is highlighted in *SI Appendix*, Fig. S9 and described in *SI Appendix*, *Text 2*. The bidirectional transformation of screw/edge-oriented dislocation originates from the generation of dislocation kinks and jogs in RMPEAs (*SI Appendix*, Figs. S7–S9) (13, 27), which causes the multiple-slip-system activation to induce dislocation multiplication (Fig. 3*C*).

In order to deeply explore the underlying mechanisms on the plastic flow of HfNbTa, the velocity field and its curl of moving screw dislocation under shear stress in a non-uniform lattice distortion field are calculated (Fig. 4A). An interesting phenomenon "dislocation flow turbulence" is observed in the severely distorted crystals, similar to a liquid turbulence (Fig. 4A). In order to compare the dislocation velocity field and fluid velocity field, the incompressible Navier–Stokes equation is combined with non-uniform lattice stress field to obtain fluid velocity field (SI Appendix, Text 1):

$$\begin{split} \frac{\partial u}{\partial t} + u \cdot \nabla u &= -\frac{1}{\rho} \nabla P + \frac{1}{\rho} \nabla \left(\mu \nabla u + \tau_{SRO} + \tau_{ext} \right) \,, \\ \nabla u &= 0 \end{split} \tag{1}$$

where τ_{SRO} is the non-uniform lattice stress obtained from SRO and lattice distortion, and τ_{ext} is the extra stress from the loading (Fig. 1*C*). The velocity field predicted by Navier–Stokes equation embedded in a non-uniform lattice stress field from MPEA is compared with the dislocation velocity field, and it shows the same statistical results for the vortex distribution (*SI Appendix*, Fig. S10). This phenomenon indicates that an unusual dislocation velocity turbulence behavior is found in severely distorted RMPEAs. Here, the solid turbulence refers to the turbulent behavior of the dislocation velocity field, while the fluid turbulence refers to the turbulent behavior of the fluid velocity field. Essentially, they are all studying the velocity field of the solid/fluid samples in the nonlinear motion

systems. To probe the existence of dislocation flow turbulence in the traditional alloys and face-centered cubic MPEAs, *SI Appendix*, Fig. S11 shows the dislocation velocity and its curl (*SI Appendix*, Tables S5 and S6). It can be found that dislocation turbulence behavior is universally present in severely distorted crystals.

Thus, when the dislocation moving horizontally at a uniform speed encounters the high strain peak obstacles (the enrichment zone of Hf and Nb in SI Appendix, Fig. S12), a vertical speed of dislocation occurs between adjacent layers, resulting in the generation of dislocation flow turbulence (Fig. 4A). This trend causes dislocations pile-up at the vortex (Fig. 4B). Surprisingly, a large number of movable and immovable dislocations simultaneously appear at the vortex (Fig. 4B). Usually, the dislocation accumulation leads to the entanglement, causing the characteristic transition from the movable dislocations to immovable dislocations (18). At the vortex point, due to the turbulent behavior of dislocations, the dislocation has a local rotational speed, resulting in a segment of spiral dislocation structure out of plane (Fig. 4B). This spiral structure serves as a source of dislocations to emit movable dislocations (Fig. 4C), which is also underlying reasons for bidirectional transformation of screw/edge-oriented dislocation (SI Appendix, Figs. S7-S9). Meanwhile, part of this structure intertwines with other dislocations to form immovable dislocations. Hence, the dislocation turbulence behavior at the vortex site induces a special spiral dislocation structure out of plane and serves both as a source and a trap (Fig. 4C), which simultaneously enhances strength and plasticity.

In summary, based on a random field theory, we propose the atomic-lattice-distortion dependent DDD simulation to reveal the underlying crystal plasticity and hardening mechanism of the collective motion of massive dislocations in severely distorted bcc crystals. Our work demonstrates the generation of edge-oriented dislocations in the initial pure screw dislocation structure is observed due to the jog formation, consistent with the experiment

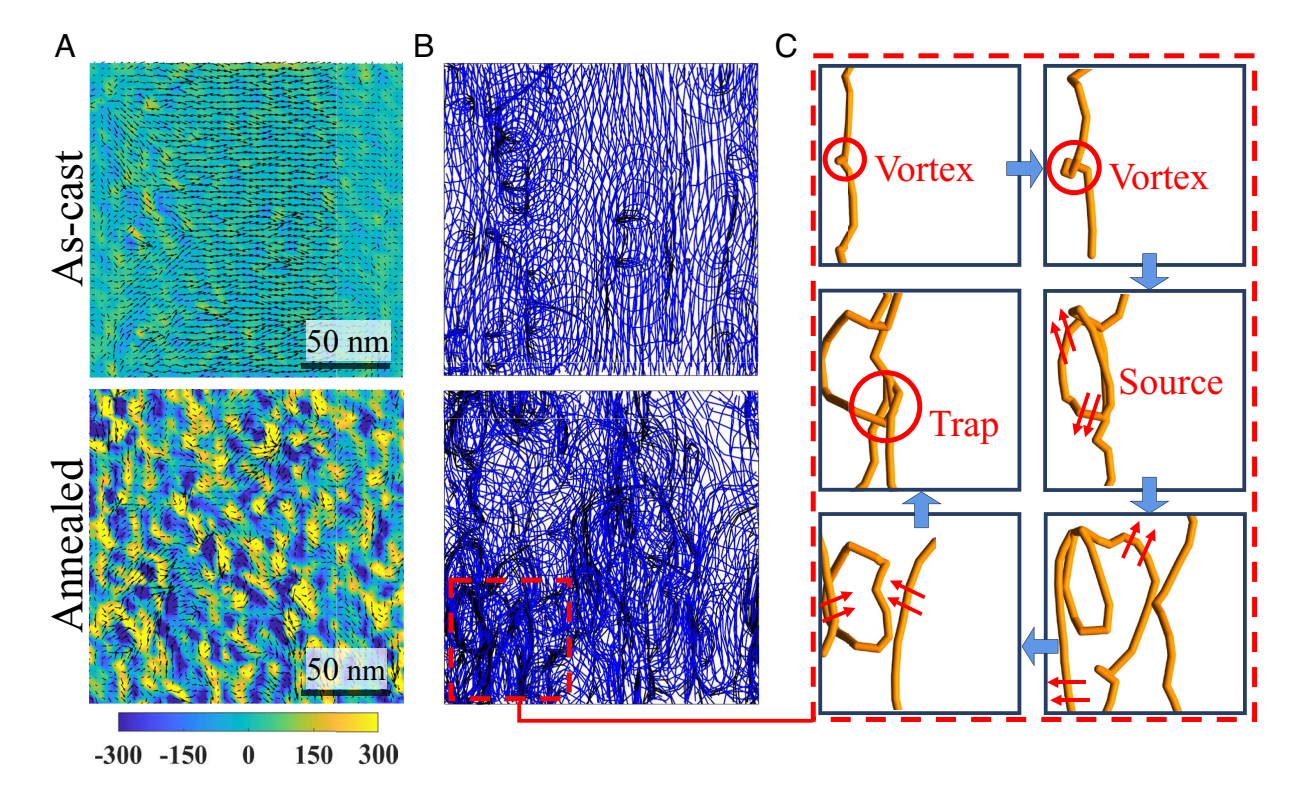


Fig. 4. Dislocation flow turbulent behavior in HfNbTa. (*A*) Dislocation velocity field of screw dislocation under constant shear stress and its curl. (*B*) The distribution of movable/immovable dislocation marked by blue/black line. (*C*) The schematic diagram for the dual role of vortex as dislocation sources and obstacles.

in RMPEAs. Importantly, a dislocation flow turbulence during the plastic deformation is observed and confirmed in the severely distorted HfNbTa by the Navier-Stokes equation, owning to the presence of strong heterogeneous lattice strain fields from SRO. The high density of movable/immovable dislocation is generated at the vortex, which enhances simultaneously strength and plasticity. This study provides a feasible approach to explore an origin of strain hardening as well as crystal plasticity and opens a path toward the development of the MPEA with superior mechanical properties by tuning the amplitude and dispersion of the heterogeneous lattice distortion.

Materials and Methods

Strain Field Calculated From Atomic Simulation. The hybrid MC/MD simulations are carried out using the large-scale atomic/molecular massively parallel simulator package (28) with the embedded atom method (EAM) potential (15), and the atomic configurations are visualized with the Ovito package (29). The simulation cells illustrated in Fig. 1A have the dimensions of 22 \times 22 \times 22 nm³ along x, y, and z directions and contain 549,250 atoms. The crystal orientations are [100], [010], and [001] directions along x, y, and z axes. A time step is 1.0 fs. First, the atomic model is relaxed and then equilibrated at the temperature of 300 K under an isothermal-isobaric (NPT) ensemble. Then, the MC step combined with MD step is conducted, where each MC step includes a swap of one random atom with another random different-type atom using Metropolis algorithm under a canonical ensemble. The samples with different SROs are prepared by the number of the cycle, where every cycle contains 10 MC swaps hybrid with 100 MD steps. Here, the as-cast and annealed samples are obtained by the number of the 0 and 500 cycles. To obtain the strain field, the software "Ovito" is applied. Here, the atomic level strain tensors are estimated based on the displacement gradient tensor of each atom corresponding to the distance from the initial configuration to the equilibrated configurations in the MD simulations. The atomic strain tensor is obtained from the dimension and shape changes and given by $\varepsilon_{ij} = (u_{i,j} + u_{j,i})/2$ (i, j = x, y, z), where ε_{ij} is 3D strain field around the atom, and u is the atomic displacement. SI Appendix, Fig. S1 shows the three-dimensional strain field maps of the annealed sample obtained from atomic simulations (Fig. 1A).

Dislocation Drag Coefficient. The dislocation mobility of both the $1/2 \langle 111 \rangle \{110\}$ edge and $1/2 \langle 11\overline{2} \rangle \{110\}$ screw dislocations in the HfNbTa RMPEA is studied. The EAM potential is employed for the descriptions of the interactions between atoms in the HfNbTa RMPEA and a time step is 1.0 fs.

- 1. Z. Li, K. G. Pradeep, Y. Deng, D. Raabe, C. C. Tasan, Metastable high-entropy dual-phase alloys overcome the strength-ductility trade-off. Nature 534, 227-230 (2016)
- Z. F. Lei et al., Enhanced strength and ductility in a high-entropy alloy via ordered oxygen complexes. Nature 563, 546-550 (2018).
- P. Koželj et al., Discovery of a superconducting high-entropy alloy. Phys. Rev. Lett. 113, 107001
- D. Liu et al., Exceptional fracture toughness of CrCoNi-based medium-and high-entropy alloys at 20 kelvin. Science 378, 978-983 (2022).
- S. Zhao et al., Amorphization in extreme deformation of the CrMnFeCoNi high-entropy alloy. Sci. Adv. 7, eabb3108 (2021).
- O. N. Senkov, D. B. Miracle, K. J. Chaput, J. P. Couzinie, Development and exploration of refractory high entropy alloys-A review. J. Mater. Res. 33, 3092-3128 (2018).
- F. L. Wang et al., Multiplicity of dislocation pathways in a refractory multiprincipal element alloy. Science 370, 95-101 (2020).
- D. Caillard, B. Bienvenu, E. Clouet, Anomalous slip in body-centred cubic metals. Nature 609, 936-941 (2022).
- E. Ma, Unusual dislocation behavior in high-entropy alloys. Scripta Mater. 181, 127-133 (2020).
- 10. X. Chen et al., Direct observation of chemical short-range order in a medium-entropy alloy. Nature **592**, 712-716 (2021).
- 11. Q. Q. Ding et al., Tuning element distribution, structure and properties by composition in high-entropy alloys. Nature 574, 223-227 (2019).
- 12. R. Zhang et al., Short-range order and its impact on the CrCoNi medium-entropy alloy. Nature 581, 283-287 (2020).
- 13. J. Ding, Q. Yu, M. Asta, R. O. Ritchie, Tunable stacking fault energies by tailoring local chemical order in CrCoNi medium-entropy alloys. Proc. Natl. Acad. Sci. U.S.A. 115, 8919-8924 (2018).

The previous investigation of dislocation mobility depending on the length of dislocation line shows that the CRSS converges when the dislocation (either edge or screw) is longer than 25 nm in the ternary RMPEAs (30). The size of the initial configuration in the RMPEA is $25.5 \times 43.7 \times 14.8 \text{ nm}^3$. The system is oriented on $x = [11\overline{2}]$, y = [111], $z = [\overline{1}10]$ for the edge dislocation and x = [111], $y = [11\overline{2}], z = [\overline{1}10]$ for the screw dislocation, and the corresponding structures are described in SI Appendix, Fig. S2 A and B. Thus, the edge/screw dislocation line length is 25.5 nm, and the dislocation line structures are shown in SI Appendix, Fig. S2 C and D. The energy minimization is performed, using the periodic-boundary conditions along x and y directions and the free boundary condition along z direction. The system is permitted to relax under a canonical (NVT) ensemble at room temperature for 100 ps. With the increasing applied shear loading, the edge/screw dislocation undergoes the obvious local movement prior to the load. The drag coefficient is obtained as the inverse of the slope by fitting the speed-stress data in the linear regime (SI Appendix, Text 1 and Fig. 1B).

DDDs Simulations. The DDD simulations are performed using ParaDiS program (31). The material parameters applied in DDD simulations are listed in SI Appendix, Table S1. Two different models are described in detail below. In the bulk DDD simulation, the cube simulation box is constructed with a size of 1.76 μm and periodic-boundary conditions, referring to the previous DDD simulation (32). Three initial dislocation structures are constructed (randomly distributed screw dislocations, randomly distributed screw and edge dislocations, and randomly distributed edge dislocations) with the initial dislocation density of 5.5 \times 10¹² m⁻², and then, they are relaxed under a no-load condition. Only the dislocation on {110} slip planes is used (27). The strain rate is set to $\dot{\varepsilon} = 10^4 \, \text{s}^{-1}$ along [001] (24). In the single screw dislocation DDD simulation, the simulation box is 180 nm with the periodic-boundary conditions. The x-axis, y-axis, and z-axis are oriented along $[1\overline{2}\overline{1}]$, $[11\overline{1}]$, and [101], respectively. The screw dislocation is under a constant shear stress of 1.6 GPa.

Data, Materials, and Software Availability. All study data are included in the article and/or SI Appendix.

ACKNOWLEDGMENTS. We would like to deeply appreciate the support from National Natural Science Foundation of China (12372069, 12302083, U2267252, and 12172123), China Postdoctoral Science Foundation (2023M731061 and BX20230109), Natural Science Foundation of Hunan Province (2022JJ20001), and the Hunan Provincial Innovation Foundation for Postgraduate (CX20220378). C.J. is grateful for the financial support from the XPLORER PRIZE and New Cornerstone Science Foundation. P.K.L. very much appreciates the support from the NSF (DMR-1611180, 1809640, and 2226508).

- 14. R. R. Eleti, N. Stepanov, N. Yurchenko, D. Klimenko, S. Zherebtsov, Plastic deformation of solid-solution strengthened Hf-Nb-Ta-Ti-Zr body-centered cubic medium/high-entropy alloys. Scripta Mater. 200, 113927 (2021).
- S. Maiti, W. Steurer, Structural-disorder and its effect on mechanical properties in single-phase TaNbHfZr high-entropy alloy. Acta Mater. 106, 87-97 (2016).
- 16. R. S. Sayles, T. R. Thomas, Surface topography as a nonstationary random process. Nature 271, 431-434 (1978).
- 17. Y.T. Shao, R. Yuan, Y. Hu, Q. Yang, J. M. Zuo, The paracrystalline nature of lattice distortion in a high entropy alloy. arXiv [Preprint] (2019). https://doi.org/10.48550/arXiv.1903.04082 (Accessed 7 June 2022).
- 18. J. Li et al., Heterogeneous lattice strain strengthening in severely distorted crystalline solids. Proc. Natl. Acad. Sci. U.S.A. 119, e2200607119 (2022).
- 19. A. Rida, E. Martinez, D. Rodney, P. A. Geslin, Influence of stress correlations on dislocation glide in random alloys. Phys. Rev. Mater. 6, 033605 (2022).
- 20. F. X. Zhang et al., Local structure and short-range order in a NiCoCr solid solution alloy. Phys. Rev. Lett. 118, 205501 (2017).
- R. B. Sills, N. Bertin, A. Aghaei, W. Cai, Dislocation networks and the microstructural origin of strain hardening. Phys. Rev. Lett. 121, 085501 (2018).
- T. Y. Thomas, Remark on a distortion tensor for elastic displacements. Proc. Natl. Acad. Sci. U.S.A. 30, 140-143 (1944).
- J. Ren et al., Strong yet ductile nanolamellar high-entropy alloys by additive manufacturing. Nature 608, 62-68 (2022).
- H. Fan, Q. Wang, J. A. El-Awady, D. Raabe, M. Zaiser, Strain rate dependency of dislocation plasticity. Nat. Commun. 12, 1845 (2021).
- R. Zhang et al., Direct imaging of short-range order and its impact on deformation in Ti-6Al. Sci. Adv. 5, eaax2799 (2019).
- 26. D. Utt et al., The origin of jerky dislocation motion in high-entropy alloys. Nat. Commun. 13, 4777 (2022).

- Y. N. Cui, G. Po, N. Ghoniem, Temperature insensitivity of the flow stress in body-centered cubic micropillar crystals. *Acta Mater.* 108, 128–137 (2016).
 S. Plimpton, Fast parallel algorithms for short-range molecular dynamics. *J. Comput. Phys.* 117, 1410 (2017).
- A. Stukowski, Visualization and analysis of atomistic simulation data with OVITO-the Open Visualization Tool. *Modell. Simul. Mater. Sci. Eng.* **18**, 015012 (2009).

- S. Xu, W. R. Jian, Y. Su, I. J. Beyerlein, Line-length-dependent dislocation glide in refractory multi-principal element alloys. *Appl. Phys. Lett.* **120**, 061901 (2022).
 V. V. Bulatov *et al.*, Dislocation multi-junctions and strain hardening. *Nature* **440**, 1174–1178 (2006).
 A. Arsenlis, M. Rhee, G. Hommes, R. Cook, J. Marian, Dislocation dynamics study of the transition from homogeneous to heterogeneous deformation in irradiated body-centered cubic iron. *Acta Mater.* **60**, 3748–3757 (2012).